Challenge Journal of Structural Mechanics

Research Article

On the evaluation of lateral-torsional buckling of web-tapered cantilevers with doubly symmetric I-section

Tolga Yılmaz [a,*], Mustafa Sertçelik [a], Hasan Selim Şengel [b]

[a] *Department of Civil Engineering, Konya Technical University, 42250 Konya, Türkiye*
[b] *Department of Civil Engineering, Eskişehir Osmangazi University, 26040 Eskişehir, Türkiye*

ABSTRACT

Recently, structural engineers have tended to design stronger and lighter structures due to economic reasons, technical developments in computer-aided design, and improvements in manufacturing. The demand for designing stronger and lighter structures has led to the compulsory considering structural efficiency and stability loss at the design level. Lateral-torsional buckling (LTB) is a major stability loss for web-tapered cantilevers with doubly symmetric I-section, which are aesthetic and structurally efficient. The elastic LTB loads of these cantilevers should be calculated at the design level since the LTB may happen before bending stress reaches yield. Studies related to the LTB of cantilevers are rare and require numerical solutions since the LTB mode shape of cantilevers is complex compared to simply supported beams. The present study introduces an analytical procedure based on the energy method for calculating elastic LTB of web-tapered cantilevers with doubly-symmetric I-section in two different forms. The analytical model considers different transverse load types, positions of loads, and web tapering degrees. The analytical solutions were validated with one-dimensional finite element analysis using a beam element. Excellent accordance between results was demonstrated. The general LTB behavior of web-tapered cantilevers with doubly symmetric I-section was clarified with detailed comments based on results obtained from the presented analytical model.

ARTICLE INFO

Article history:
Received 22 August 2023
Revised 10 November 2023
Accepted 1 December 2023

Keywords:
Lateral-torsional buckling
Web-tapered cantilevers
Finite element analysis
Analytical method

1. Introduction

Steel web-tapered cantilevers with I-section are very popular structural members by means of aesthetic features and light weights. A good optimization could be achieved by tapering their web along the cantilever length considering the variation of bending moment. In other words, web height is maximum at fixed support, and it decreases towards to free end since the bending moment is lowered too. However, a web-tapered cantilever bending about its major axis may buckle out of a plane by deflecting laterally and twisting for a level of the applied transverse load. This stability loss is called lateral-torsional buckling (LTB), and the critical load level where buckling occurs is elastic LTB load (Yilmaz 2023). Fig. 1 depicts the LTB of a cantilever. The elastic LTB load of beams, beam-columns, and cantilevers subjected to uniform bending can be calculated by solving related differential equations; however, analytical solutions may be very complex or include infinite series when moment distributions vary along the length of the structural member and/or structural member has support conditions differ from simple support (Yilmaz and Kirac 2017; Yilmaz et al. 2017, 2019; Yilmaz 2023). At this point, numerical methods such as finite differences (Ozbasaran 2013; Ozbasaran 2014; Assasi and Roeder 1985) and finite integral (Anderson and Trahair 1972; Kitipornchai et al. 1984) were utilized for the calculation of the elastic LTB load of cantilevers. Based on the finite element solutions performed, Xiao et al. (2023) derived practical equations to calculate the elastic LTB load of doubly symmetric cantilevers for essential load cases.

* *Corresponding author*. Tel.: +90-332-205-1500 ; Fax: +90-332-241-0635 ; E-mail address: tyilmaz@ktun.edu.tr (T. Yılmaz)
ISSN: 2149-8024 / DOI: https://doi.org/10.20528/cjsmec.2023.04.004

Nomenclature

A_i , B_i	The amplitudes of the buckled mode shape
b_f	Top and bottom flanges' width
C	Center of gravity
$C_w(z)$	The warping constant
$d(z)$	Heights of cross-section
E	Young's modulus
G	Shear modulus
$h(z)$	Heights of web
$h_0(z)$	The distance between flange centers
h_i	The height of the web at the fixed end
H_p	Vertical distance between the shear center and load application points for the point load
H_q	Vertical distance between the shear center and load application points for the distributed load
$I_y(z)$	The moment of inertia belonging to the weak axis
$J(z)$	Torsional constant
$M_x(z)$	The bending moment about the major axis
P	Point load
q	Distributed load
S	Shear center
t_f	Top and bottom flanges' thickness
u	Lateral displacement of the shear center
U	The strain energy stored in the cantilever
v	Vertical displacement of the shear center
V	The work done by the external transverse forces
V_M	Additional work done by the end moment acting on shear center
Π	The total potential energy of the cantilever
φ	Torsion rotation of the shear center
Φ_L	The free-end rotation
Φ_p	Torsional rotation at the application point of the point load

The energy method, which is based on the equality between the additional strain energy stored when LTB occurs and the additional work done by the applied forces, is a favorable approach to evaluating elastic LTB of steel structural members. To determine elastic LTB load with this method, a buckled shape that represents the actual mode shape and provides kinematic boundary conditions is substituted in the total potential equation belonging to the slightly buckled position (Yilmaz 2023; Trahair 1993). While closed-form equations for beam and beam-columns could be established using the energy method with basic mode shapes, it is hard or commonly impossible to generate equations for cantilevers due to their complex mode shape (Yilmaz 2023). The energy method was used to calculate the elastic LTB of beams, beam-columns, and castellated beams (Mohri et al. 2008; Kim et al. 2016; Torkamani and Roberts 2009; Yilmaz et al. 2017; Ozbasaran 2019; Saoula et al. 2021; Bresser et al. 2020; Belaid et al. 2018; Pham 2022). Furthermore, the LTB load of the beams with mono-symmetric I-sections (Yilmaz and Kirac 2017; Yilmaz et al. 2019; Mohri et al. 2003; Mohri et al. 2013; Aydin et al. 2015; Mohammadi et al. 2016), the beams with various cross sections such as C, Z and box (Cheng et al. 2013; Saoula et al. 2016; Zhang and Tong 2016), and cantilevers (Wang and Kitipornchai 1986; Ozbasaran et al. 2015; Andrade et al. 2007; Aydin et al. 2013; Zhang and Tong 2008; Zhang et al. 2016; Yilmaz 2023) were evaluated utilizing the energy method.

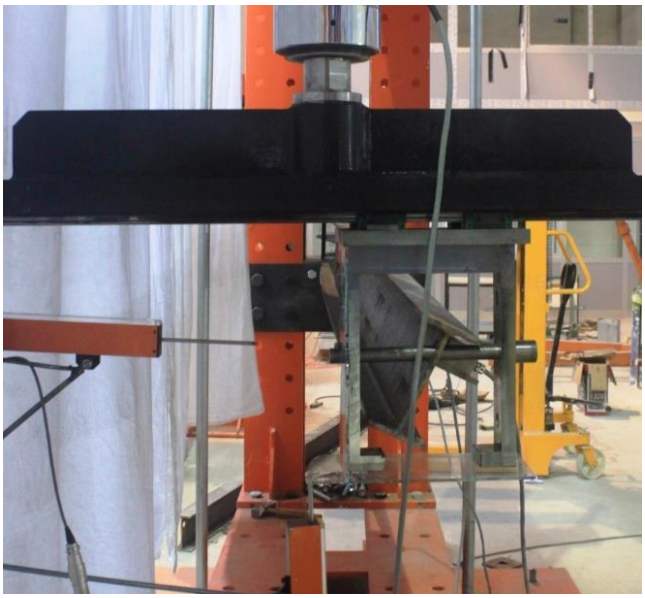

Fig. 1. The LTB of a cantilever.

Experimentally and analytical investigation on the stability of web or flange tapering beams with doubly symmetric and mono-symmetric I-sections were presented in studies by Kitipornchai and Trahair (1972) and Kitipornchai and Trahair (1975). Trahair (2017) developed a treatment based on the finite element method for calculating the LTB of tapered beam-columns, which is subjected to various load types and has different boundary conditions. Benyamina et al. (2013) developed a formula for LTB of web-tapered beams with doubly symmetric I-section. The LTB of beams with arbitrary cross-sections was studied by Asgarian et al. (2013). The LTB of the beams, of which flanges and web simultaneously tapered, was investigated by the study of Kus (2015). Trinh et al. (2023) introduced an approximate expression to evaluate the critical moment of simply supported I-section beams whose height changes. Osmani and Meftah (2018) presented a study focused on the LTB of symmetric beam-columns considering shear deformations. Yuan et al. (2013) studied the LTB of T-section cantilevers. The LTB of web-tapered mono-symmetric I-section cantilevers were examined by Andrade et al. (2007) and Andrade and Camotim (2005). In these comprehensive analytical studies, pre-buckling effects have been included in the energy method, and numerical LTB examples for beams and cantilevers subjected to point load were presented. It should be emphasized that elastic LTB load must be calculated with the above-mentioned methods and considered in design since LTB may occur before the bending stress of the cross-section's extreme fibre comes to yield.

The literature review conducted reveals that there is no comprehensive study related to the LTB of cantilevers

with doubly-symmetric I-section exposed to different load cases by considering their positions along the cross-section. The primary motivation of the present study is to establish an analytical procedure based on the energy method, which is easily programmable with mathematical software, to determine the elastic LTB load of web-tapered cantilevers with doubly-symmetric I-section for six load cases and three loading positions which are top and bottom flange and shear center loadings. The analytical results were compared to one-dimensional finite element analysis (1D-FEA) using LTBeamN software. In light of the results of numerical examples, slenderness and tapering effects were interpreted, and explanations were presented. The study will contribute to understanding the uncharted LTB behaviour of web-tapered symmetric I-section cantilevers with detailed interpretations as well as the analytical procedure that enables the calculation of critical LTB load for the design of steel members.

2. Analytical Procedure

In the present study, the analytical model has been developed for web-tapered cantilevers with symmetric I-section, which have two different tapering forms illustrated in Fig. 2. In the first of two tapering forms, depicted in Fig. 2(a), web tapering has been provided by the obliquity of the bottom flange while the top flange is parallel to the cantilever's longitudinal z-axis. In the second form, illustrated in Fig. 2(b), web tapering has been provided by the obliquity of both the top and bottom flanges. In the study, cantilevers with the first tapering form will be named Cantilever Type 1 ($C1$), and Cantilever Type 2 ($C2$) will be used for the cantilevers with the second tapering form. Before the LTB occurs, the cantilever bends about its major axis under the effects of transverse loads, and then the cantilever buckles by deflecting laterally and twisting, shown in Fig. 2(c), when the magnitude of the loads reaches the elastic critical LTB load.

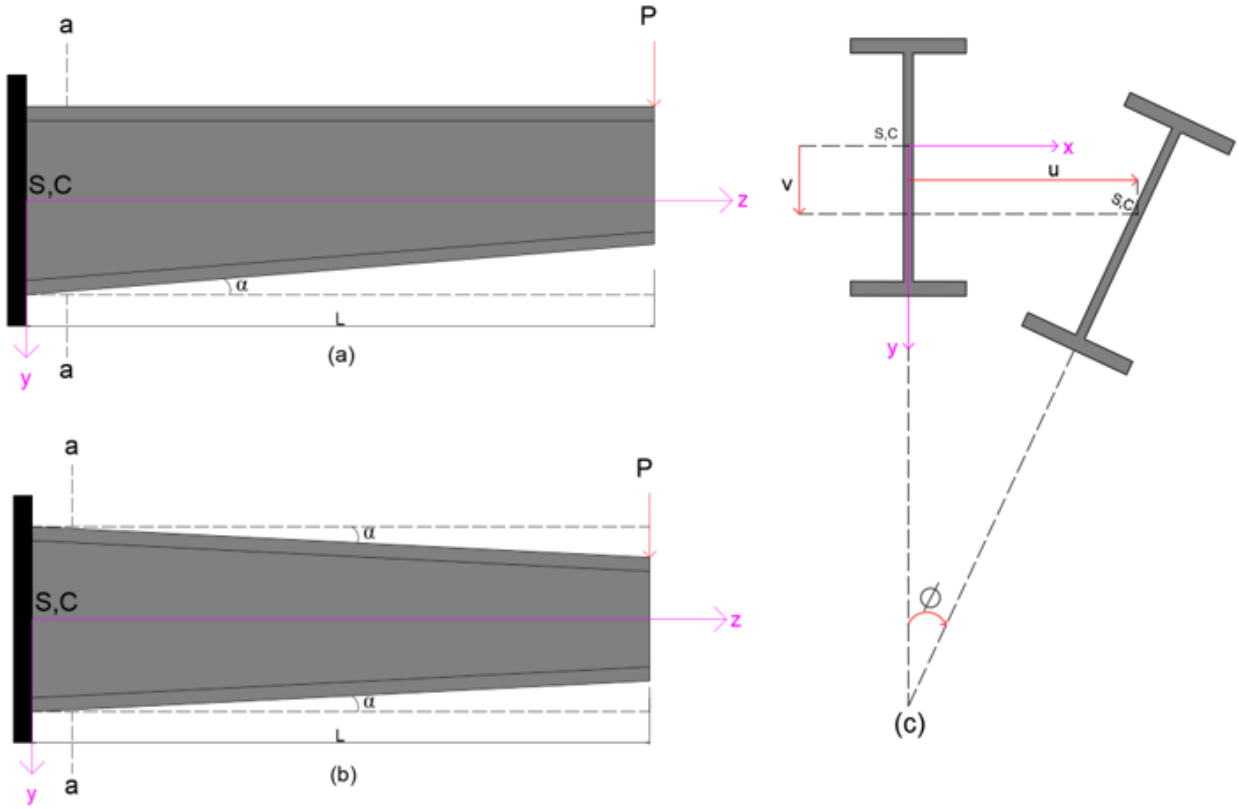

Fig. 2. The LTB of web-tapered cantilevers.

In Fig. 2(a), α and L are the tapering angle and the cantilever length, respectively. Fig. 2(c) illustrates the a-a section of the web-tapered cantilevers. In Fig. 2, while the S and C denote the shear center and the center of gravity, respectively, the lateral and vertical displacements and the torsional rotation of the shear center were given with u, v, and φ, respectively. Fig. 3 shows the cross-section dimensions of a web-tapered cantilever with a doubly symmetric I-section. In Fig. 3, while the top and bottom flange width is shown with b_f, the t_f denotes the top and bottom flanges' thickness. The d and h are heights of cross-section and web, respectively.

These two dimensions depend on the distance to the fixed end in the z-axis since h decreases with tapering. The height (h) can be expressed for the $C1$ and $C2$ cantilevers as given in Eqs. (1) and (2), respectively.

$$h(z) = h_i - z * \tan(\alpha) \tag{1}$$

$$h(z) = h_i - 2 * z * \tan(\alpha) \tag{2}$$

where h_i refers to the height of the web at the fixed end. Therefore d becomes:

$$d(z) = h(z) + 2 * t_f \tag{3}$$

The warping constant $C_w(z)$, torsional constant $J(z)$, and the moment of inertia belonging to the weak axis

$I_y(z)$ are the main parameters which effective on the LTB. For a web-tapered cantilevers in Fig. 2, $C_w(z)$, $J(z)$, and $I_y(z)$ can be expressed as follows:

$$C_w(z) = \frac{h_0^2(z) b^3 t_f}{24} \tag{4}$$

$$J(z) = \frac{2bt_f{}^3 + h_0(z) t_w^3}{3} \tag{5}$$

$$I_y(z) = \frac{2b^3 t_f + h(z) t_w^3}{12} \tag{6}$$

where the $h_0(z)$ is the distance between flange centers and given as follows:

$$h_0(z) = d(z) - t_f = h(z) + t_f \tag{7}$$

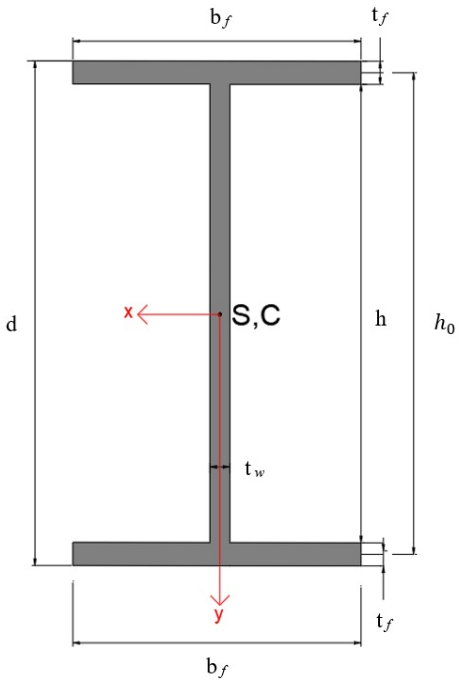

Fig. 3. The cross-section dimensions of the doubly symmetric I-section.

The strain energy stored in the cantilever due to lateral bending, warping, and torsion, respectively, can be written as follows (Yilmaz 2023; Yilmaz et al. 2019):

$$U = \frac{1}{2}\int_0^L EI_y(z)\left[\frac{d^2u(z)}{dz^2}\right]^2 dz + \frac{1}{2}\int_0^L EC_w(z)\left[\frac{d^2\phi(z)}{dz^2}\right]^2 dz + \frac{1}{2}\int_0^L GJ(z)\left[\frac{d\phi(z)}{dz}\right]^2 dz \tag{8}$$

where E and G are Young's modulus and shear modulus, respectively. The work done by the external transverse forces can be expressed as in Eq. (9) (Yilmaz 2023; Yilmaz et al. 2019):

$$V = \frac{1}{2}\int_0^L M_x(z)\left[2\phi(z)\left[\frac{d^2u(z)}{dz^2}\right]\right] dz + \frac{1}{2}\sum PH_p\phi_p^2 + \frac{1}{2}\int_0^L qH_q\phi(z)^2 dz + M\phi_L\left[\frac{du_L}{dz}\right] \tag{9}$$

where $M_x(z)$ implies the bending moment about the major axis. The works of point load P and distributed load q, acting out of the shear center, were taken place as second and third terms in Eq. (9). The source of these works is the variation of distance between the application point of loads and shear center during rotation of section. H_p and H_q denote the vertical distance between the shear center and load application points for P and q, respectively. H_p and H_q should be taken as positive when the load application point is below the shear center. The Φ_p shows torsional rotation at the application point of the point load.

Furthermore, an external moment acting on the shear center at the end of the cantilever generates additional work existing in the last term of Eq. (9). To understand this additional work V_M, end moment M is replaced with an equivalent force couple, which are in opposite directions and acts on flange centers. These forces displace relatively in longitudinal directions, leading to additional work when the cross-section rotates. V_M can be calculated by multiplying the magnitude of forces with their displacement in the longitudinal direction as follows (Yilmaz 2023):

$$V_M = 2\left[\frac{M}{h_0(L)}\right]\left[h_0(L)\frac{\emptyset_L}{2}\frac{du_L}{dz}\right] = M\phi_L\left[\frac{du_L}{dz}\right] \tag{10}$$

In Eq. (10), Φ_L is the free-end rotation. Eventually, the total potential energy (Π=U+V) of the cantilever can be expressed as in Eq. (11) by considering Vlassov's model. In this model, the cross-section is rigid in its plane, and the shear deformation belonging to the section's mean surface can be neglected (Yilmaz 2023).

$$\Pi = \frac{1}{2}\int_0^L EI_y(z)\left[\frac{d^2u(z)}{dz^2}\right]^2 dz + \frac{1}{2}\int_0^L EC_w(z)\left[\frac{d^2\phi(z)}{dz^2}\right]^2 dz + \frac{1}{2}\int_0^L GJ(z)\left[\frac{d\phi(z)}{dz}\right]^2 dz + \frac{1}{2}\int_0^L M_x(z)\left[2\phi(z)\left[\frac{d^2u(z)}{dz^2}\right]\right] dz + \frac{1}{2}\sum PH_p\phi_p^2 + \frac{1}{2}\int_0^L qH_q\phi(z)^2 dz + M\phi_L\left[\frac{du_L}{dz}\right] \tag{11}$$

The energy method predicates the equality of the strain energy stored due to the effect of LTB and the external forces' work. The energy method necessitates a buckled mode function representing the real buckled shape and providing boundary conditions that constrain deflection and/or rotations at supports. At fixed support of the cantilevers, all deflections and rotations are zero. Therefore, u, ϕ, du/dz, $d\phi/dz$ are taken as zero at fixed support. The u, ϕ, du/dz, $d\phi/dz$ are unconstrained at the free end. The cantilever mode shape can be defined as lateral deflection (u) and rotation angle (Φ), which belongs to the shear center. Bearing in mind above mentioned restrain conditions for cantilevers, the buckled mode function can be implied as in Eqs. (12) and (13). The amplitudes of the buckled mode shape were shown as A_i and B_i.

$$u(z) = \sum_{i=1}^{n} A_i\left(\frac{z}{L}\right)^{i+1} \tag{12}$$

$$\phi(z) = \sum_{i=1}^{n} B_i\left(\frac{z}{L}\right)^{i+1} \tag{13}$$

When buckled shape functions are substituted in Eq. (11), the total potential energy becomes as follows:

$$\Pi = U + V = f(A_1, A_2, A_3 \dots, A_n, B_1, B_2, B_3 \dots, B_n) \quad (14)$$

The 2n variables of the total potential energy function are A_i and B_i. The LTB occurs when the total energy function reaches a stationary condition, which can be expressed with the following equations:

$$\frac{\partial \Pi}{\partial A_i} = 0 \quad \text{for } i = 1,2 \dots n \quad (15)$$

$$\frac{\partial \Pi}{\partial B_i} = 0 \quad \text{for } i = 1,2 \dots n \quad (16)$$

Eqs. (15) and (16) yield a system of 2n homogeneous linear equations, which can be expressed as follows:

$$[K]_{2nx2n} \{d\}_{2nx1} = \{0\}_{2nx1} \quad (17)$$

where K is a coefficient matrix and $\{d\} = \{A_1, A_2, A_3 \dots, A_n, B_1, B_2, B_3 \dots, B_n\}^T$. Eq. (17) has been satisfied when the determinant of the K coefficient matrix equals zero.

$$\det [K]_{2nx2n} = 0 \quad (18)$$

Eq. (18) yields a power series of order 2n, whose smallest feasible root gives the elastic LTB load or moment. The present analytical treatment can be easily programmed utilizing mathematical software such as Matlab, Mathematica, Mathcad, etc. The current analytical treatment can enable for calculation LTB load of both web-tapered cantilevers depicted in Fig. 2 under various load types considering their positions along the cross-sections.

3. Numerical Analysis

In the numerical analysis, based on the analytical model introduced, the elastic LTB loads of both web-tapered cantilevers $C1$ and $C2$ were calculated for six different load cases, presented in Fig. 4, and three loading positions, which are top flange, bottom flange, and shear center loadings. The end-moment loading was applied only on the shear center. The cantilevers' lengths and tapering angles were taken as variables to investigate the effects of the tapering and the slenderness on the LTB of $C1$ and $C2$ cantilevers. The section properties of cantilevers used in numerical analysis are given in Table 1. Names of cantilevers consist of four characters, the first two of which shows cantilever types $C1$ and $C2$, and the rest of two imply specimen number from $S1$ to $S11$. The d_e denotes the height of the cross-section at the free end. All dimensions in Table 1 are in units of mm. The tapering angles are in units of degree. The untapered cross-section was in dimensions of IPN-200, commonly used in structural practice. However, fillets were neglected, and flange thickness was assumed to be constant. The cantilever length was appropriate for the slender section assumption, considering crudely L/h>5. Similar cantilever lengths were used in previous works (Yilmaz 2023; Andrade and Camotim 2005). Previous studies argued that the energy method based on beam element assumption might not precisely reflect the LTB behavior of very compact sections and demonstrated the requirement for 3D finite element analysis (Yilmaz 2023; Andrade and Camotim 2005). Tapering angles were chosen to prevent excessive tapering at the free end according to the initial by considering manufacturing. Cantilever tapering was designed so that the cross-section height at the free end was not less than 50% of the height at the fixed end.

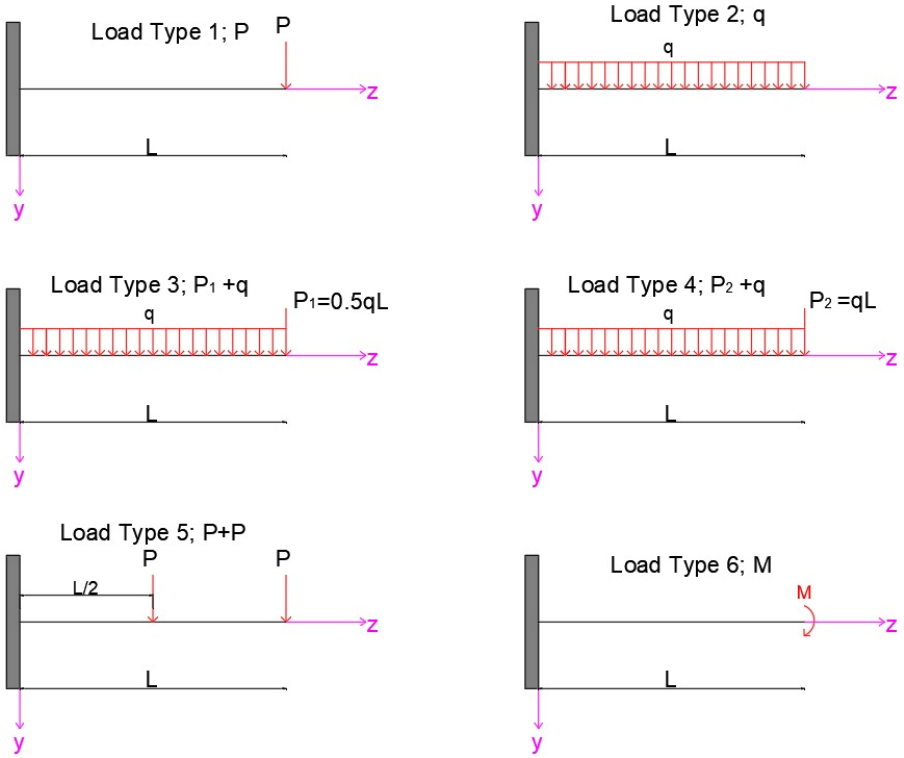

Fig. 4. The considered load types in the numeric analysis.

In the numerical analysis, the elastic modulus and Poisson's ratio were taken as $2 \cdot 10^5$ MPa and 0.3, respectively. All elastic buckling loads calculated via the presented analytical method were compared with the 1D finite element analysis (1D-FEA) using LTBeamN software (Centre Technique Industriel de la Construction Metallique 2015). LTBeamN software has been commonly used to solve elastic LTB problems in the literature (Yilmaz 2023; Kucukler and Gardner 2019; Yilmaz et al. 2017, 2019; Yilmaz and Kirac 2017; Kovac 2012). The software calculates the elastic LTB load analysis utilizing the beam elements that consider warping. LTBeamN allows users to define almost any common open section. Users can define sections using a pre-defined catalog or modifying dimensions for various cross-sections that are commonly used. Furthermore, sections may be defined by using their section properties that are effective in buckling. Users may change section height through its length to allow the analysis of haunched and tapered sections and assemble members from different upper and lower sections. The software provides flexibility for defining restraint conditions.

Table 1. The section properties of cantilevers used in the numerical analysis.

Variables	Sections	α	L	d	d_e	b_f	t_f	t_w
Tapering angles	C1S1	0	3000	200	200	90	11.3	7.5
	C1S2	0.955	3000	200	150	90	11.3	7.5
	C1S3	1.909	3000	200	100	90	11.3	7.5
	C2S4	0.477	3000	200	150	90	11.3	7.5
	C2S5	0.955	3000	200	100	90	11.3	7.5
Slenderness	C1S6	1.273	3000	200	133.34	90	11.3	7.5
	C1S7	1.273	3500	200	122.23	90	11.3	7.5
	C1S8	1.273	4000	200	111.12	90	11.3	7.5
	C2S9	0.637	3000	200	133.34	90	11.3	7.5
	C2S10	0.637	3500	200	122.23	90	11.3	7.5
	C2S11	0.637	4000	200	111.12	90	11.3	7.5

Restrain positions can be defined for any position both along the cross-section and length of the member. For each restraint, four different degrees of freedom can be defined. External and internal loading options can be used for loading structural members. In the external loading, concentrated and distributed loads can be added to the demanded positions along the cross-sections and length of the member. A bending diagram and axial load should be provided for buckling analysis in the internal loading. Besides, a self-weight of member may be added as an option. LTBeamN presents numerical results and graphical output to determine buckling loads and modes. Furthermore, the software has yielded compatible results with 3D finite element analysis (3D-FEA), where solid and shell elements are used (Yilmaz 2023; Yilmaz et al. 2017, 2019; Yilmaz and Kirac 2017). The numerical analysis results were presented in Tables 2-7 for six load cases respectively. These tables include elastic LTB loads of all cantilevers presented in Table 1 for top and bottom flange loadings and also shear center loadings. In the tables, AN and LT denote the elastic LTB loads obtained using the present analytical model and LTBeamN software. R implies the ratio of the analytical model results to the LTBeamN results.

Table 2. Load case 1, P_{cr} (kN).

	Top flange			Shear center			Bottom flange		
Cantilevers	AN	LT	R	AN	LT	R	AN	LT	R
C1S1	22.53	21.85	1.03	32.20	31.67	1.02	38.36	37.89	1.01
C1S2	24.41	23.69	1.03	31.53	31.03	1.02	36.31	35.82	1.01
C1S3	26.34	25.84	1.02	30.87	30.49	1.01	34.19	33.81	1.01
C2S4	24.41	23.69	1.03	31.53	31.03	1.02	36.31	35.82	1.01
C2S5	26.34	25.84	1.02	30.87	30.50	1.01	34.19	33.81	1.01
C1S6	25.06	24.39	1.03	31.31	30.84	1.02	35.61	35.14	1.01
C1S7	18.54	18.11	1.02	21.79	21.44	1.02	24.16	23.81	1.01
C1S8	14.19	13.88	1.02	16.00	15.73	1.02	17.39	17.12	1.02
C2S9	25.06	24.39	1.03	31.31	30.84	1.02	35.61	35.15	1.01
C2S10	18.55	18.11	1.02	21.79	21.44	1.02	24.15	23.81	1.01
C2S11	14.19	13.88	1.02	16.00	15.73	1.02	17.39	17.12	1.02

Table 3. Load case 2, q_{cr} (kN/m).

	Top flange			Shear center			Bottom flange		
Cantilevers	AN	LT	R	AN	LT	R	AN	LT	R
C1S1	24.78	24.11	1.03	39.86	39.23	1.02	53.75	53.12	1.01
C1S2	26.41	25.02	1.06	39.11	38.50	1.02	51.01	50.64	1.01
C1S3	28.20	26.17	1.08	38.36	37.87	1.01	48.16	48.26	1.00
C2S4	26.41	25.01	1.06	39.11	38.50	1.02	51.02	50.69	1.01
C2S5	28.21	26.16	1.08	38.36	37.88	1.01	48.16	48.36	1.00
C1S6	26.99	25.38	1.06	38.86	38.28	1.02	50.08	49.83	1.00
C1S7	17.08	16.11	1.06	22.86	22.49	1.02	28.34	28.21	1.00
C1S8	11.46	10.83	1.06	14.52	14.27	1.02	17.45	17.36	1.00
C2S9	26.99	25.36	1.06	38.85	38.29	1.01	50.07	49.91	1.00
C2S10	17.09	16.10	1.06	22.86	22.50	1.02	28.34	28.24	1.00
C2S11	11.46	10.82	1.06	14.52	14.27	1.02	17.44	17.38	1.00

When results presented in Tables 2-7 are examined, it has been found that the present analytical approach excellent matches with the 1D-FEA solutions performed with LTBeamN. Results demonstrated that the present analytical approach has been successful in capturing the effects of tapering level and slenderness on the LTB of web-tapered cantilevers. The average difference between analytical and numerical results is only 2%, and the maximum difference very rarely reaches 8% for compact sections where the energy method exhibits slightly worst performance on evaluation of the LTB since it bases on a beam element assumption. As slenderness increases, the beam element assumption becomes more valid; consequently, the energy method yields better accordant buckling loads with the FEA results. Similar tendencies were observed in previous studies (Yilmaz 2023; Yilmaz et al. 2019; Yilmaz and Kirac 2017).

It should be noted here that for short cantilevers, a more exact evaluation of the LTB may be achieved with 3D-FEA with shell element instead of the energy method based on 1D frame element assumption since the remarkable web and/or flange distortion or a localized web buckling phenomenon taking place near the application point of load is not captured with the 1D frame element assumption (Yilmaz 2023; Andrade et al. 2007; Ozbasaran et al. 2015).

It should be remembered that, as mentioned above, choosing a proper buckling mode shape reflecting the actual buckling mode is critical to the performance of the energy method. In the analytical calculations, sixth-order functions were used in Eqs. (12) and (13); in other words, n=5 was taken. With the increase of n, the difference between analytical and numerical results may be lowered. However, it must not be remembered that higher-order functions considerably increase computational time.

Table 4. Load case 3, $q_{cr}+0.5q_{cr}\cdot L$ (kN/m).

	Top flange			Shear center			Bottom flange		
Cantilevers	AN	LT	R	AN	LT	R	AN	LT	R
C1S1	9.53	9.26	1.03	14.18	13.95	1.02	17.90	17.68	1.01
C1S2	10.25	9.86	1.04	13.90	13.68	1.02	16.93	16.78	1.01
C1S3	11.01	10.57	1.04	13.61	13.45	1.01	15.93	15.91	1.00
C2S4	10.25	9.86	1.04	13.90	13.68	1.02	16.93	16.79	1.01
C2S5	11.01	10.57	1.04	13.61	13.45	1.01	15.93	15.93	1.00
C1S6	10.50	10.09	1.04	13.80	13.60	1.01	16.60	16.49	1.01
C1S7	6.65	6.41	1.04	8.19	8.06	1.02	9.54	9.47	1.01
C1S8	4.45	4.30	1.04	5.24	5.15	1.02	5.95	5.90	1.01
C2S9	10.50	10.09	1.04	13.80	13.60	1.01	16.60	16.49	1.01
C2S10	6.65	6.40	1.04	8.19	8.06	1.02	9.54	9.48	1.01
C2S11	4.45	4.29	1.04	5.24	5.15	1.02	5.95	5.91	1.01

Table 5. Load case 4, q_{cr}+q_{cr}·L (kN/m).

	Top flange			Shear center			Bottom flange		
Cantilevers	AN	LT	R	AN	LT	R	AN	LT	R
C1S1	5.85	5.68	1.03	8.56	8.42	1.02	10.58	10.45	1.01
C1S2	6.31	6.09	1.04	8.38	8.25	1.02	10.00	9.90	1.01
C1S3	6.78	6.57	1.03	8.21	8.11	1.01	9.41	9.37	1.00
C2S4	6.30	6.09	1.04	8.38	8.25	1.02	10.01	9.91	1.01
C2S5	6.78	6.57	1.03	8.21	8.11	1.01	9.41	9.38	1.00
C1S6	6.46	6.24	1.04	8.33	8.20	1.02	9.81	9.72	1.01
C1S7	4.09	3.97	1.03	4.95	4.87	1.02	5.66	5.61	1.01
C1S8	2.74	2.66	1.03	3.17	3.12	1.02	3.55	3.51	1.01
C2S9	6.46	6.24	1.04	8.33	8.20	1.01	9.81	9.73	1.01
C2S10	4.09	3.97	1.03	4.95	4.87	1.02	5.66	5.61	1.01
C2S11	2.74	2.66	1.03	3.17	3.12	1.02	3.55	3.51	1.01

Another critical finding revealing the general LTB behavior of web-tapered cantilevers, obtained from the numerical study, is that increases in tapering level, or other words, the tapering angles, have led to a decrease in elastic LTB loads for all load cases applied to the shear center and bottom flange. However, when transverse loads are acted on top flanges of web-tapered cantilevers, the LTB loads have increased with the increase of tapering. This unexpected result, less material providing more strength, can be explained by two opposite effects due to the increase in tapering. The first of these effects is the decrease in stiffness due to the rise in tapering. This effect causes a reduction in buckling load, as expected. The second effect stems from the decline in the distance between the application point of the transverse load and the shear center when tapering increases. In contrast to the first effect, this effect leads to a rise in buckling load. Consequently, since the second effect is more dominant, the elastic LTB load has increased when the load is applied to the top flange with the increase in tapering. It can be explicitly observed that these two effects tend to decrease buckling load with the increase of tapering when transverse loads are applied to the bottom flange. Therefore, for bottom flange loading, the increase in tapering cause a decrease in the LTB loads.

Table 6. Load case 5, P_{cr}+P_{cr} (kN).

	Top flange			Shear center			Bottom flange		
Cantilevers	AN	LT	R	AN	LT	R	AN	LT	R
C1S1	19.25	18.68	1.03	29.00	28.51	1.02	37.38	36.90	1.01
C1S2	20.72	20.13	1.03	28.44	27.96	1.02	35.36	34.87	1.01
C1S3	22.23	21.81	1.02	27.87	27.51	1.01	33.26	32.86	1.01
C2S4	20.72	20.13	1.03	28.44	27.96	1.02	35.37	34.87	1.01
C2S5	22.23	21.81	1.02	27.87	27.51	1.01	33.26	32.87	1.01
C1S6	21.22	20.68	1.03	28.25	27.81	1.02	34.67	34.20	1.01
C1S7	15.67	15.08	1.04	19.56	19.29	1.01	23.19	23.11	1.00
C1S8	11.99	11.71	1.02	14.30	14.04	1.02	16.49	16.22	1.02
C2S9	21.22	20.68	1.03	28.25	27.81	1.02	34.67	34.20	1.01
C2S10	15.67	15.30	1.02	19.56	19.23	1.02	23.19	22.84	1.02
C2S11	11.99	11.72	1.02	14.30	14.04	1.02	16.49	16.23	1.02

4. Conclusions

The present study has established an analytical treatment to evaluate the lateral-torsional buckling behavior of web-tapered doubly symmetric I-section cantilevers. In the scope of the study, two different forms of cantilevers, of which web tapering is created by the obliquity of only the bottom flanges and both top and bottom flanges.

The analytical model considers the variation of moment distribution, the position of transverse load along the cross-section, and the tapering level. Thus, cantilevers were investigated under six load cases and three loading positions in numerical analysis. The LTB loads obtained by the analytical method were compared to 1D finite element analysis.

It has been found that there is only, on average, a 1%

difference between numerical and analytical LTB loads. An increase in tapering caused a decrease in the LTB loads when the transverse load was applied to the bottom flange and shear center; however, the opposite tendency occurred for top flange loadings. The increase in tapering has brought along two opposite effects, which are effective on the LTB of web-tapered cantilevers subjected to top flange loading. The first is a decrease in stiffness, which cause a reduction in buckling loads, and the second is a decrease in the distance between the application point of loads and the shear center, leading to an increase in buckling load. For top flange loading, since the second effect is more dominant, the LTB loads have increased when tapering increased.

Table 7. Load case 6, M_{cr} (kN·m).

	Shear center		
Cantilevers	AN	LT	R
C1S1	26.62	25.96	1.03
C1S2	25.91	24.93	1.04
C1S3	25.18	24.15	1.04
C2S4	25.91	24.93	1.04
C2S5	25.18	24.16	1.04
C1S6	25.67	24.64	1.04
C1S7	21.70	20.88	1.04
C1S8	18.77	18.11	1.04
C2S9	25.67	24.64	1.04
C2S10	21.70	20.88	1.04
C2S11	18.77	18.11	1.04

Author Contributions

All of the authors made substantial contributions to conception and design, or acquisition of data, or analysis and interpretation of data; were involved in drafting the manuscript or revising it critically for important intellectual content; and gave final approval of the version to be published.

Acknowledgements

The present study results are based on a section that exists in the Master of Science thesis, which Mustafa Sertçelik has been being prepared at the Graduate Education Institute, Konya Technical University. Dr. Tolga Yılmaz is a supervisor of the thesis.

Funding

The authors received no financial support for the research, authorship, and/or publication of this manuscript.

Conflict of Interest

The authors declared no potential conflicts of interest with respect to the research, authorship, and/or publication of this manuscript.

Data Availability

The datasets created and/or analyzed during the current study are not publicly available, but are available from the corresponding author upon reasonable request.

REFERENCES

Anderson JM, Trahair NS (1972). Stability of monosymmetric beams and cantilevers. *Journal of Structural Division*, 98(ST1), 269-86.

Andrade A, Camotim D (2005). Lateral–torsional buckling of singly symmetric tapered beams: Theory and applications. *Journal of Engineering Mechanics*, 131, 586–597.

Andrade A, Camotim D, Dinis PB (2007). Lateral-torsional buckling of singly symmetric web-tapered thin-walled I-beams: 1D model vs. shell FEA. *Computers and Structures*, 85, 1343–1359.

Andrade A, Camotim D, Providência e Costa P (2007). On the evaluation of elastic critical moments in doubly and singly symmetric I section cantilevers. *Journal of Constructional Steel Research*, 63, 894-908.

Asgarian B, Soltani M, Mohri, F (2013). Lateral-torsional buckling of tapered thin-walled beams with arbitrary cross-sections. *Thin-Walled Structures*, 62, 96-108.

Assadi M, Roeder CW (1985). Stability of continuously restrained cantilevers. *Journal of Engineering Mechanics*, 111(12), 1440–1456.

Aydin, R, Gunaydin A, Kirac N (2015). On the evaluation of critical lateral buckling loads of prismatic steel beams. *Steel and Composite Structures*, 18(3), 603-621.

Aydin R, Ozbasaran H, Kirac N, Gunaydin A (2013). Lateral torsional buckling of double angle and tee cantilevers: A parametric study. *Proceedings of the Fourteenth International Conference on Civil, Structural and Environmental Engineering Computing*, Civil-Comp Press, Stirlingshire, Scotland.

Belaid T, Ammari F, Adman R. (2018). Influence of load position on critical lateral torsional buckling moment of laterally restrained beam at tense flange. *Asian Journal of Civil Engineering*, 19, 839–48.

Benyamina AB, Meftah, S., Mohri F, Daya EM (2013). Analytical solutions attempt for lateral torsional buckling of doubly symmetric web-tapered I-beams. *Thin-Walled Structures*, 56, 1207-1219.

Bresser D, Ravenshorst GJP, Hoogenboom PCJ. (2020). General formulation of equivalent moment factor for elastic lateral torsional buckling of slender rectangular sections and I-sections. *Engineering Structures*, 207, 110-230.

Kim B, Li L, Edmonds A (2016). Analytical solutions of lateral-torsional buckling of castellated beams. *International Journal of Structural Stability and Dynamics*, 16, 155044.

Kitipornchai S, Dux PF, Richter NJ (1984). Buckling and bracing of cantilevers. *Journal of the Structural Division*, 110 (9), 2250-2262.

Kitipornchai S, Trahair NS (1972). Elastic stability of tapered I-beams. *Journal of the Structural Division*, 98(ST3), 713–728

Kitipornchai S, Trahair NS (1975). Elastic behaviour of tapered monosymmetric I-beams. *Journal of the Structural Division*, 101(ST8), 1661–1678

Kováč M. (2012). Lateral-torsional buckling of web-tapered I-beams 1D and 3D FEM approach. *Procedia Engineering*, 40, 217–22.

Kucukler M, Gardner L. (2019). Design of web-tapered steel beams against lateral-torsional buckling through a stiffness reduction method. *Engineering Structures*, 190, 246–61.

Kus J (2015). Lateral-torsional buckling steel beams with simultaneously tapered flanges and web. *Steel and Composite Structures*, 19(4), 897–916.

LTBeamN (2015). Centre Technique Industriel de la Construction Metallique.

Mohammadi E, Hosseini SS, Rohanimanesh SM (2016). Elastic lateral-torsional buckling strength and torsional bracing stiffness requirement for monosymmetric I-beams. *Thin-Walled Structures*, 104, 116-125.

Mohri F, Bouzerira C, Potier-Ferry M (2008). Lateral buckling of thin-walled beam-column elements under combined axial and bending loads. *Thin-Walled Structures*, 46(3), 290–302.

Mohri F, Brouki A, Roth JC (2003). Theoretical and Numerical Stability Analyses of Unrestrained, Mono-Symmetric Thin-Walled Beams. *Journal of Constructional Steel Research*, 59(1), 63-90.

Mohri F, Damil N, Potier-Ferry M (2013). Buckling and lateral buckling interaction in thin-walled beam-column elements with mono-symmetric cross sections. *Applied Mathematical Modelling*, 37(5), 3526–3540.

Osmani A, Meftah SA (2018). Lateral buckling of tapered thin walled bi-symmetric beams under combined axial and bending loads with shear deformations allowed. *Engineering Structures*, 165, 76–87.

Ozbasaran H (2013). Finite differences approach for calculating elastic lateral torsional buckling moment of cantilever I sections. *Anadolu University Journal of Science and Technology- A- Applied Science and Engineering*, (2), 143–152.

Ozbasaran H (2014). A parametric study on the evaluation of lateral torsional buckling of European IPE and IPN beams. *World Academy of Science, Engineering and Technology International Journal of Civil and Environmental Engineering*, 8(7), 783-788.

Ozbasaran H (2019). Convergence of the Rayleigh–Ritz Method for buckling analysis of arbitrarily configured I-section beam–columns. *Archive of Applied Mechanics*, 89, 2397–414.

Ozbasaran H, Aydın R, Dogan M (2015). An alternative design procedure for lateral-torsional buckling of cantilever I-beams. *Thin-Walled Structures*, 90, 235-242.

Pham PV (2022). An innovated theory and closed form solutions for the elastic lateral torsional buckling analysis of steel beams/columns strengthened with symmetrically balanced GFRP laminates. *Engineering Structures*, 256, 114-046.

Saoula A, Meftah SA, Mohri F, Daya EM (2016). Lateral buckling of box beam elements under combined axial and bending loads. *Journal of Constructional Steel Research*, 116, 141-155.

Saoula A, Selim MM, Meftah SA, Benyamina AB, Tounsi A (2021). Simplified analytical method for lateral torsional buckling assessment of RHS beams with web openings. *Structures*, 34, 2848–60.

Torkamani MAM, Roberts ER (2009). Energy equations for elastic flexural-torsional buckling analysis of plane structures. *Thin-Walled Structures*, 47(4), 463-473.

Trahair NS (1993). Flexural-Torsional Buckling of Structures. CRC Press, London, UK.

Trahair NS (2017). Lateral buckling of tapered members. *Engineering Structures*, 151, 518–26.

Trinh DK, Nguyen DH, Bui HC, Nguyen MT (2023). Lateral torsional buckling of I-section simply supported beams with stepped height. *Steel Construction*, 16, 1-6.

Wang CM, Kitipornchai S (1986). On stability of monosymmetric cantilevers. *Engineering Structures*, 8, 168-180.

Xiao G, Ho S, Papangelis JP (2023). Semi analytical solutions for flexural-torsional buckling of thin-walled cantilever beams with doubly symmetric cross-sections. *Structural Engineering and Mechanics*, 87, 541-554.

Yilmaz T (2023). Rapid evaluation of lateral-torsional buckling of European standard I-section cantilevers. *Mechanics Based Design of Structures and Machines*.

Yilmaz T, Kirac N (2017). Analytical and parametric investigations on lateral torsional buckling of European IPE and IPN beams. *International Journal of Steel Structures*, 17, 695–709.

Yilmaz T, Kirac N, Anil Ö (2019). An alternative evaluation of the LTB behavior of mono-symmetric beam-columns. *Steel and Composite Structures*, 30, 471–81.

Yilmaz, T, Kirac N, Kilic T (2017). Lateral-torsional buckling of european wide flange I-section beams. *Proceedings of the 2nd World Congress on Civil Structural and Environmental Engineering* (*CSEE'17*).

Yuan W, Kim B, Chen C (2013). Lateral-torsional buckling of steel web tapered tee-section cantilevers, *Journal of Constructional Steel Research*, 87, 31–37.

Zhang L, Tong GS (2016). Lateral buckling of simply supported C- and Z-section purlins with top flange horizontally restrained. *Thin-Walled Structures*, 99, 155-167.

Zhang L, Tong GS (2008). Elastic flexural-torsional buckling of thin-walled cantilevers. *Thin-Walled Struct*ures, 46, 27–37.

Zhang WF, Liu YC, Hou GL, Chen KS, Ji J, Deng Y (2016). Lateral-torsional buckling analysis of cantilever beam with tip lateral elastic brace under uniform and concentrated load. *International Journal of Steel Structures*, 16, 1161–73.